Journal of Power Sources 227 (2013) 211–217

Contents lists available at SciVerse ScienceDirect

Journal of Power Sources

journal homepage: www.elsevier.com/locate/jpowsour

Surface and structural stabilities of carbon additives in high voltage lithium ion batteries

Jianming Zheng, Jie Xiao*, Wu Xu, Xilin Chen, Meng Gu, Xiaohong Li, Ji-Guang Zhang*

Pacific Northwest National Laboratory, Richland, WA 99354, USA

HIGHLIGHTS

- We investigate different carbon additives in high voltage lithium ion batteries.
- We examine the surface and structural stability of different carbons during charge to high voltage.
- Increasing surface area will increase irreversible capacity and reduce long-term cycling stability.
- Surface functional groups will be oxidized at high voltage and leads to poor cycling stability.

ARTICLE INFO

Article history:
Received 23 August 2012
Received in revised form
18 October 2012
Accepted 14 November 2012
Available online 23 November 2012

Keywords:
Carbon additive
Irreversible capacity
Functional group
High voltage
Lithium ion battery
Energy storage

ABSTRACT

The stabilities of different conductive carbon additives have been systematically investigated in high voltage lithium ion batteries. It is found that the higher surface area of conductive additives leads to more parasitic reactions initiating from different onset voltages. A closer inspection reveals that for the low surface area carbon such as Super P, PF_6^- anions reversibly intercalate into carbon structure at around 4.7 V. For high surface area carbons, in addition to the electrolyte decomposition, the oxidation of functional groups at high voltage further increases the irreversible capacity and Li^+ ion consumption. Coulombic efficiency, irreversible capacity and cycling stability observed by using different carbon additives are correlated with their structure and surface chemistry, thus providing information for predictive selection of carbon additives in different energy storage systems.

1. Introduction

Conductive carbon additives, such as acetylene black (AB) [1,2], Super P (SP) [3–5], Super C [1], usually have relatively low surface area and pore volume and are often used during the preparation of battery electrodes to improve their electronic conductivity. Other high surface area carbon, for example, Ketjen black (KB) contains mesoporous carbon structure with high pore volume [6]. Therefore, when used as carbon additive, less amount of KB is required to achieve similar electronic conductivity of the whole electrode [7,8]. Recently, graphene has also emerged as a conductive medium for the development of high performance lithium ion battery due to its high electronic conductivity and large surface area [9–11]. All of these non-active carbon additives can provide a continuous conductive network among active materials and facilitate fast current flow through the entire electrode, improving the utilization rate of active materials and reducing the polarization effects [12]. In addition, carbon additives could also absorb and retain the electrolyte solution, which increases the intimate contact between electrolyte and active materials [13]. These additives usually work well for conventional Li-ion batteries operating at a voltage below 4.4 V, but their electrochemical behaviors at a voltage above 4.4 V are rarely studied systematically.

In this work, the electrochemical properties of several commonly used carbon additives were investigated in a voltage range required for high-energy Li-ion batteries (>4.4 V) using high voltage spinel $LiNi_{0.5}Mn_{1.5}O_4$ as a platform. High voltage spinel $LiNi_{0.5}Mn_{1.5}O_4$ is considered as one of the most promising cathode materials for lithium ion battery due to its high energy density (~658 W h kg^{-1}), good cycling performance and good rate capability [3,14–18]. However, the high operating voltage of

* Corresponding authors. Tel.: +1 509 375 4598; fax: +1 509 372 2186.
E-mail addresses: jie.xiao@pnnl.gov (J. Xiao), jiguang.zhang@pnnl.gov (J.-G. Zhang).

0378-7753/$ – see front matter © 2012 Elsevier B.V. All rights reserved.
http://dx.doi.org/10.1016/j.jpowsour.2012.11.038

$LiNi_{0.5}Mn_{1.5}O_4$ (4.7 V vs. Li/Li^+) requests a rescreening of all 'inactive' components including electrolyte composition, separator, and carbon additives in the electrode. The properties of electrolyte [16], cell cans and separators [18] at high voltages have been reported earlier from this group. Here the surface and structural stabilities of different carbon additives at high voltage are discussed in detail.

2. Experimental

2.1. Preparation of material

$LiNi_{0.5}Mn_{1.5}O_4$ was synthesized according to the procedure reported previously [3]. In brief, $LiNi_{0.5}Mn_{1.5}O_4$ was prepared by ball milling the mixture of Li_2CO_3, NiO and $MnCO_3$ (All from Aldrich) in stoichiometric amount for 4 h followed by calcination at 900 °C for 24 h in air with heating rate of 10 °C min^{-1} and cooling rate of 3 °C min^{-1}. The X-ray diffraction (XRD) pattern of the prepared $LiNi_{0.5}Mn_{1.5}O_4$ could be indexed according to a cubic spinel structure, space group Fd-3m (JCPDS card no. 80-2162) [17].

2.2. Characterization

Surface area, porosity, and pore size of different carbon additives, including SP (Timcal), AB (MTI Corp.), graphene (Vorbeck Materials) and KB (Akzo Nobel Corp.), were analyzed by Brunauer–Emmett–Teller (BET) and Barrett–Joyner–Halenda (BJH) methods using a QUANTACHROME AUTOSORB 6-B gas sorption system. Morphology of spinel electrodes with different carbon additives was observed with a FEI Helios scanning electron microscope (SEM). The Raman spectra measurement was performed by a home-build Raman spectrometer which used 514.5 nm wavelength, 15 mW power excitation from an Ar ion laser to focus on the sample and collect the back-scattered Raman light [21]. Ex-situ XRD of cycled electrodes was carried out on Rigaku Miniflex II and the XRD data was collected from 10 to 90° in 2θ at a step size of 0.05°.

Carbon electrodes were prepared by coating the slurries of mixtures consisting of 80 wt% carbon and 20 wt% poly(vinylidene fluoride) (PVDF, Kynar HSV900, Arkema Inc.) binder in *N*-methylpyrrolidone (NMP) onto Al foils. Cathode electrodes were prepared by a similar approach with a mixture containing 80 wt% $LiNi_{0.5}Mn_{1.5}O_4$, 10 wt% carbon additive, and 10 wt% PVDF binder. After evaporating NMP, the electrodes were punched into disks with $\varnothing = 1.27$ cm and dried completely under vacuum. The active material loading was 3–5 mg cm^{-2}. CR2032 coin-type cells were assembled with the electrodes as-prepared, metallic lithium foil as counter electrode, Celgard K1640 monolayer polyethylene (PE) membrane as separator and 1 M $LiPF_6$ dissolved in ethyl carbonate (EC) and dimethyl carbonate (DMC) (1:2 in volume) as electrolyte in an argon-filled MBraun glove box. The electrochemical performance tests were performed galvanostatically between 3.2 and 5.0 V on an Arbin BT-2000 battery tester at room temperature (22–23 °C). 1 C rate corresponds to a current density of 147 mA g^{-1}. Linear scan voltammetry (LSV) of different Li|carbon cells was performed on a CHI 6005D electrochemical station (from CH Instruments) between 3 and 6 V at a scan rate of 0.1 mV s^{-1}. Electrochemical impedance spectra (EIS) measurements were performed using a CHI 6005D electrochemical station in a frequency range of 100 kHz–10 mHz.

3. Results and discussion

The surface areas of the four carbon additives investigated in this work increase in the order of: SP < AB < graphene < KB (Table 1). The LSV curves of these pure carbons plotted in Fig. 1a show very different electrochemical behaviors. For SP and AB with relatively low surface area, the onset oxidation current occurs at ca. 4.65 V, while for graphene (C/O = 100 representing the relative content of oxygen functional groups) and KB, the onset oxidation current evolves at a much lower voltage (~3.7 V). This is understandable since higher surface area provides more reaction sites for electrolyte decomposition and lowers the electrochemical window. Similar effects have been observed during recharging Li–O_2 batteries in which the air electrode is mainly composed of carbon [22–25]. In addition, high surface area carbons may catalyze the decomposition of electrolyte solvents, which has been reported in battery systems operated even below 4.5 V [26,27].

Table 1
Comparison of different carbon additives.

	Super P	Acetylene black	Graphene	Ketjen black
Surface area (m^2 g^{-1})	76.4	123.6	890–1120	1576
Pore volume (cm^3 g^{-1})	0.36	0.53	~6.2	4.86
First cycle efficiency at 0.1 C rate (%)	83.4	77.0	56.3	18.3
Capacity retention rate of spinel electrodes containing different carbon additives after 200 cycles (1 C) (%)	91.5	96.1	86.9	77.3

During anodic scan to a voltage higher than 4.5 V, accelerated electrolyte decomposition occurs as indicated by the fast increase of oxidation current for all carbons in Fig. 1a. Interestingly, one small current peak at 4.87–4.90 V is clearly observed for SP and AB, which may be related with PF_6^- intercalation into the carbon structures [19,20]. The electrochemical intercalation of PF_6^- is used in dual carbon batteries while the capacity from PF_6^- insertion is dependent on the graphitic degree of carbon [19,20,28]. Above 4.90 V, both SP and AB show continuous increase of current density while graphene and KB exhibit a maximum current between 5 and 6 V. The decrease of oxidation current on graphene and KB may be attributed to the thick passivation layer formed on those carbon surfaces, which reduces the electrolyte access to the interior carbons. Accordingly, further electrolyte decomposition on graphene and KB electrodes is prevented, as reflected by the decrease of response current after ca. 5.4 V. In other words, although KB and graphene have much higher surface area than AB and SP, the utilization rate of carbon surfaces on the former may be less than that of the latter if the electrodes are dominated by carbon (Fig. 1a). However, if carbons are used as additives and diluted in the cathodes, the utilization rate of surface areas is largely improved and will be discussed later in this work.

Carbon electrodes consisting of the four different carbons were then further investigated in cells using lithium metal as the anode. The electrochemical behaviors of these carbons in Fig. 1 strongly suggest that carbon additive, supposed to be inactive, becomes electrochemically active at high voltage. For AB and SP, small plateaus at ca. 4.7–4.8 V, corresponding to PF_6^- intercalation, are identified consistent with the LSV results (Fig. 1b). Further charging AB and SP to above 4.8 V witnesses a fast capacity increase indicating that, even on low surface area carbons, electrolyte decomposition is unavoidable at high voltages and needs to be carefully controlled. The initial charge capacity increases with increasing carbon surface area as shown in Fig. 1c. For KB with the highest surface area among the four carbon additives, an extremely high capacity of 2223 mAh g^{-1} can be reached when charged to 5.1 V. Obviously, this high capacity largely exceeds the theoretical value of intercalation chemistry in KB (~140 mAh g^{-1}) assuming a reaction product of $(PF_6)_{0.5}C_8$ [19,28]. Similar behaviors are

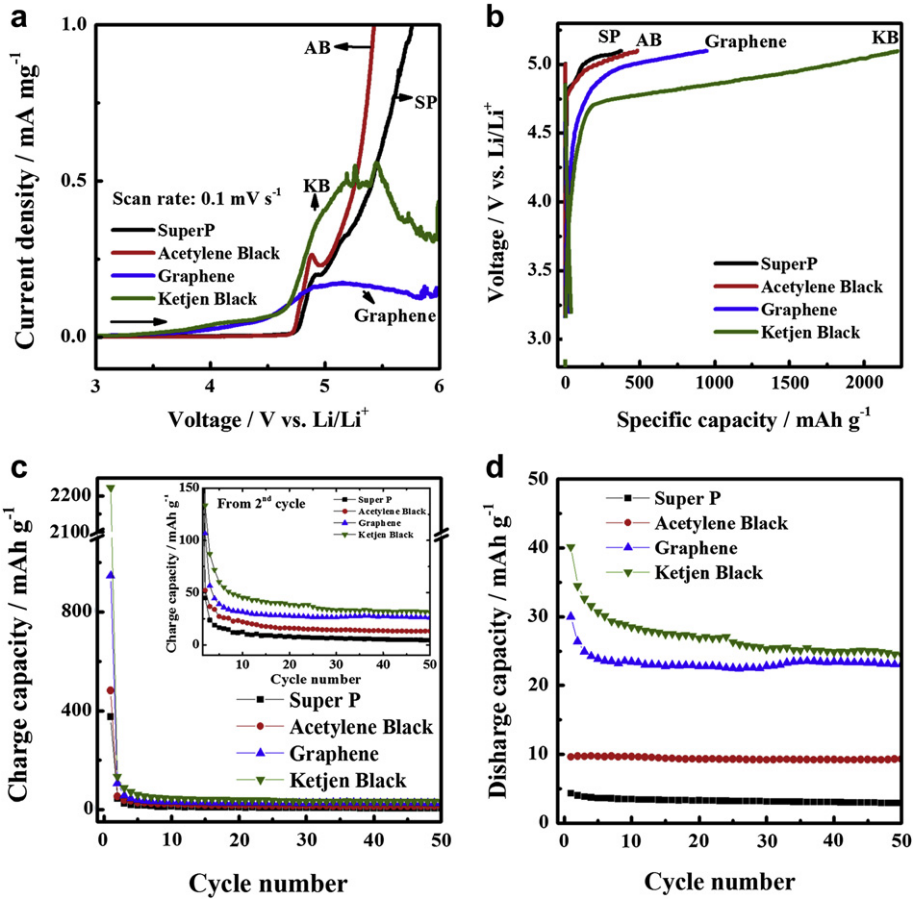

Fig. 1. (a) LSV curves of different carbon electrodes in Li|C cells at a scan rate of 0.1 mV s^{-1}. (b) First-cycle charge profiles of various carbon electrodes at 120 mA g^{-1}. Corresponding (c) charge and (d) discharge capacity during cycling at a voltage range of 3.2–5.1 V.

observed for graphene electrode in Fig. 1b and c. For these two high surface area carbons, during the initial cycling, there is a large gap between charge and discharge capacities (Fig. 1c and d), due to the parasitic reactions on carbon surfaces charged at high voltages [26,27]. In the subsequent cycling, significant decrease of charge capacities corresponds to a reduction of side reactions. Two reasons can be assigned: one is the gradual isolation of the electrode surface by passivation film that prevents further electrolyte decomposition. The other is the gradual decrease of the functional groups on carbon surface, another contributor to parasitic reactions.

Fig. 1d shows that discharge capacities from graphene and KB fade gradually while SP and AB maintain quite stable reversible capacities. The observed "discharge capacity" demonstrated by graphene or KB in Fig. 1d seems reversible. However, compared with cycling stability of SP or AB, capacity fluctuation from graphene or KB is clearly seen in Fig. 1d along with the fast capacity decay. Therefore, it is highly suspected that a large amount of the observed capacity is from continuous "irreversible" side reactions especially for the first few cycles. For SP and AB, however, reversible intercalation/deintercalation of PF_6^- into/out of carbon structures provides a quite stable cycling performance, though the degree of anion insertion is very limited as reflected by the low capacity. In real batteries, the amount of carbon additives is usually a small portion of the electrode (<10%). Therefore, capacities from SP or AB can be ignored. However, for other high surface carbonaceous additives, the greatly amplified side reactions will largely affect the cell performances and will be discussed in detail.

To further evaluate the functions of different carbon additives in lithium ion batteries, the above four carbons were mixed with high voltage spinel $LiNi_{0.5}Mn_{1.5}O_4$ [3] to form cathode electrodes for performance evaluation. SEM images of spinel electrodes with different carbon additives are shown in Fig. 2. It is well known that homogeneous dispersion between carbon additive and active material is very important to achieve good battery performance [7,8]. When super P and AB are used as carbon additives (Fig. 2a and b), active materials show uniform distribution in the whole electrodes. Graphene and KB tend to flocculate easily during the preparation of electrode slurry due to their high surface area. An extended mixing time still can lead to a well-mixed slurry that transits to a uniform electrode with spinel particles being wrapped in the graphene nanosheets or within KB pores (Fig. 2c and d).

Because $LiNi_{0.5}Mn_{1.5}O_4$ employed in this work is in micron size with low surface area ($\sim$1.4 m^2 g^{-1}) [3], electrolyte decomposition on spinel particles itself is not a major concern at high voltages [16]. Therefore, the as-prepared micron-sized spinel provides a good platform to evaluate the carbon additives in the high voltage environment. In all cases, carbon contents are fixed to be 10 wt% of the cathodes for consistence. The electrochemical performances of the carbon additives in high voltage cathodes are compared in Fig. 3. All the charge–discharge curves show typical features of high voltage spinel [3,15], except prolonged plateaus above 4.8 V for electrodes using graphene and KB additives (Fig. 3a). The large initial charge capacity from cathodes containing high surface area carbons can be assigned to side reactions between electrolyte and carbon surfaces, which generate a large amount of undesired

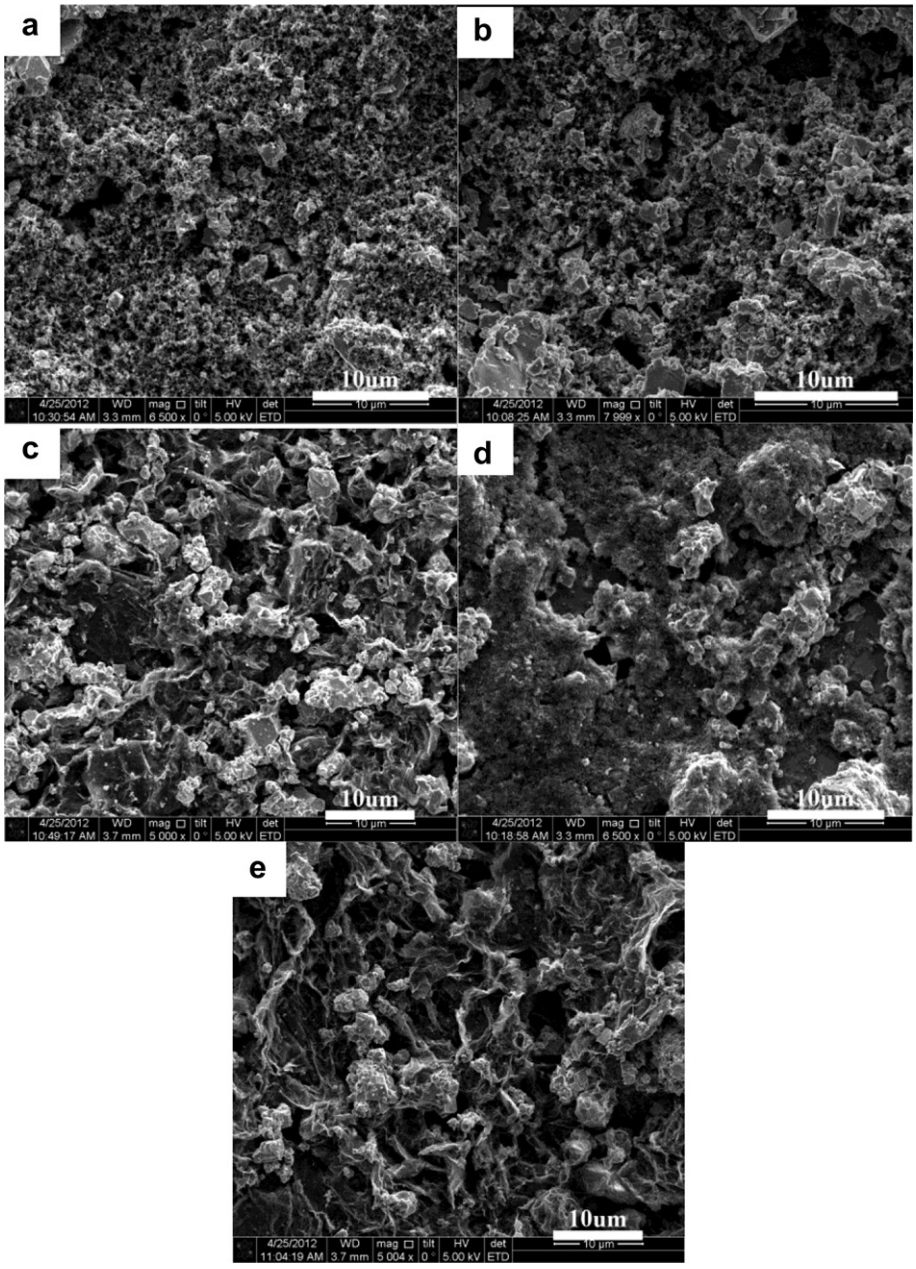

Fig. 2. SEM images of spinel electrodes with different carbon additives, (a) super P; (b) AB; (c) graphene (C/O = 100); (d) KB; (e) graphene (C/O = 14).

byproducts such as lithium carbonates and alkyl lithium carbonates [15]. Electrodes containing SP or AB exhibit much lower initial charge capacity of 145 and 154 mAh g^{-1}, respectively, close to the theoretical values of the spinels. The order of the charge capacity of the spinel cathodes with different carbon additives is also consistent with that of carbon surface areas in Table 1, indicating that high surface carbons, even as low as 10 wt% in the whole electrodes, still significantly affects the first charge process of lithium ion batteries at high voltages.

In fact, graphene and KB are usually used to enhance the performance of conventional cathode materials, such as $LiCoO_2$ and $LiNi_{1/3}Co_{1/3}Mn_{1/3}O_2$, through the increase of point-to-point (or even point-to-plane for graphene) of contact between active material and carbon additive [7,11]. For conventional cathodes $LiCoO_2$ and $LiNi_{1/3}Co_{1/3}Mn_{1/3}O_2$, the upper charge cut-off voltage is lower than 4.4 V, so the negative effect from the high surface area carbons could not be obviously observed. However, for high voltage spinel, the electrode needs to be charged to 4.9 V or above to fully utilize its reversible capacity. During slow charge to 5.0 V at 0.1 C, aggressive side reaction, mainly oxidation of electrolyte solvents EC/DMC, occurs between the carbon additive and the electrolyte. As a consequence, the first-cycle Coulombic efficiencies for spinel electrodes with graphene and KB are only 56.3%, and 18.3%, respectively (Table 1, Fig. 3b). The present results show that high surface area carbon additives used in the traditional cathodes cannot be directly applied to high voltage applications. Hidden behind the low efficiency is the fact that Li^+ ions are continuously consumed to form all kinds of salts from parasitic reactions [24]. Those parasitic reactions occurring during charge are irreversible, leading to the significantly larger charge capacity and thus lower Columbic efficiency especially in the first cycle [Fig. 3a and b]. Although the cycling performance at 0.1 C of all cathodes

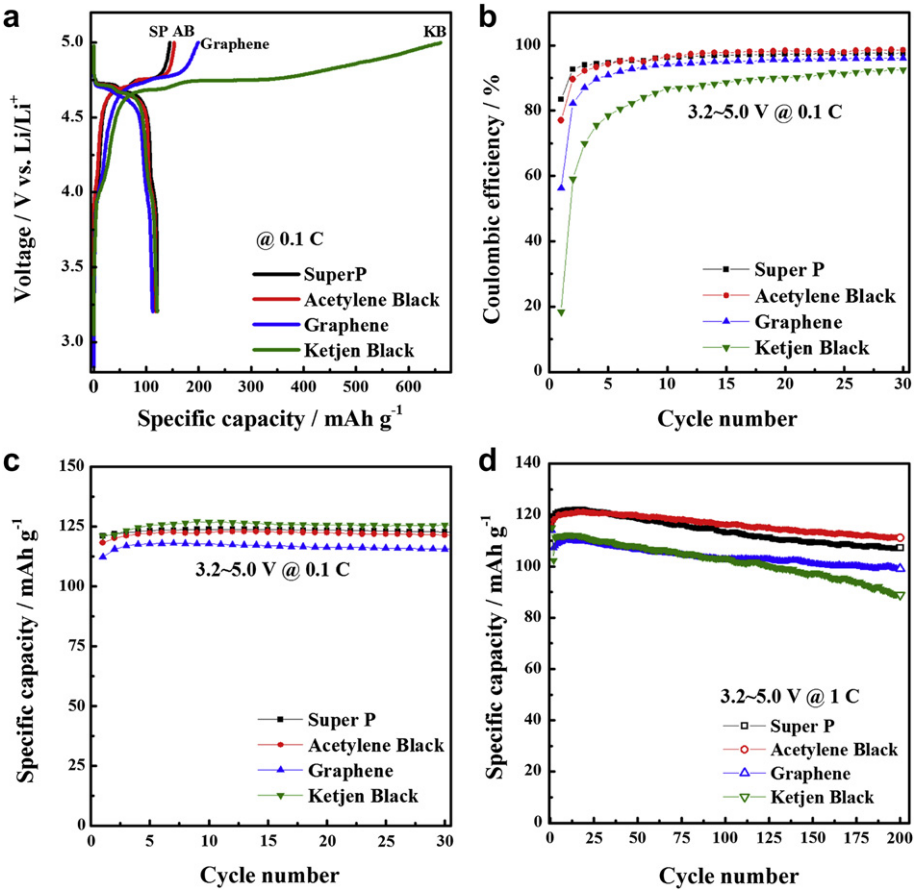

Fig. 3. (a) First-cycle charge–discharge profiles of $LiNi_{0.5}Mn_{1.5}O_4$ with various carbon additives at 0.1 C. Corresponding (b) Coulombic efficiency and (c) discharge capacity during cycling at 0.1 C. (d) Long-term cycling stability of spinel electrode with various carbon additives at 1 C.

containing different carbons (Fig. 3c) is still satisfactory due to the excess lithium source available in the lithium half-cell used in this work, the large first-cycle capacity loss shown in Fig. 3 may lead to significant capacity fade in the full cells because of the limited amount of total Li^+ ions [29–31].

The negative effects from high surface area and functional groups at high voltages can be further illustrated in Fig. 3d that compares the long-term cycling stability of the cathodes. Electrodes containing graphene and KB decay faster than those containing SP and AB (Table 1). For example, only 89 mAh g^{-1} of discharge capacity is maintained for cathode with KB additive, corresponding to 77.3% of capacity retention after 200 cycles. The most stable cycling is found to be the one with AB additive exhibiting 96.1% capacity retention after 200 cycles, which also has the highest efficiency at 1 C rate in the first cycle. Because Li^+ source is in excess amount in all of these half cells and the same active material is used, the main reason for the cycling differences could be ascribed to the interfacial reactions between high surface area carbon and electrolyte, which continuously deplete the limited amount of electrolyte in the cells. The consumed Li^+ ions along with the decomposed solvents build up thick passivation film on the electrode. Not only Li^+ migration is slowed down by this insulating film, but also the accumulation of this passivation layer may lead to the loss of electrical contact among active material, carbon additives and current collectors, greatly affecting the whole cell performances.

The highest reversible capacity of 127 mAh g^{-1} is observed in cathode using KB additive (Fig. 3c). This can be attributed to the increased contact area between active particles and high surface area KB, which improves the utilization rate of the spinel cathode material. However, the electrode containing graphene delivers the lowest capacity, even though the surface area of graphene is much higher than SP and AB. This can be explained by the existence of functional groups on graphene surface. The functional groups will be continuously oxidized at high voltage, further accelerating the passivation process and hindering the reversible Li^+ diffusion process within the whole electrode. While it is hard to quantify the number of the functional groups on KB, because KB involves disordered structure and poorly defined surface chemistry, comparison of graphene with relatively different amount of functional groups is more feasible simply by using different C/O ratio graphenes [22,32]. The C/O ratio reflects the relative content of oxygen functional groups on the graphene sheets. The smaller the C/O ratio, the more functional groups are on graphene substrates. Therefore, the electrochemical performances of spinel electrodes containing different graphenes, graphene100 (C/O = 100) and graphene14 (C/O = 14), are compared in Fig. 4.

In spite of the similar charge curves, the spinel-graphenene14 electrode shows larger IR drop during discharge (Fig. 4a). The result reveals a lowering of electrical conductivity of graphene14 during initial charge to high voltage of 5.0 V. The electrode with graphene14 shows very poor cycling stability as compared to electrode with graphene100 containing less amount of functional groups (Fig. 4b). Considering that the active material particles can intermix well with both graphene additives (Fig. 2c and e), the influence from electrode homogeneity could be ruled out. Ex-situ

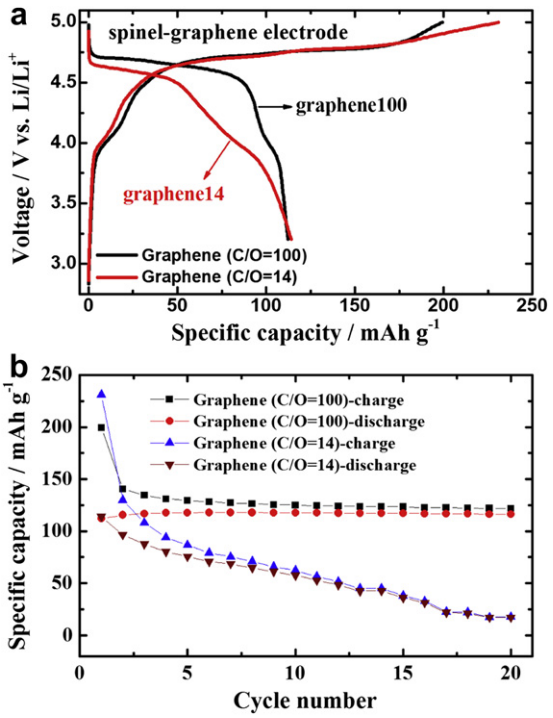

Fig. 4. (a) Initial charge–discharge profiles and (b) corresponding cycling stability of spinel electrode using graphenes with different C/O ratio (C/O = 100 and 14) as conductive additive.

XRD also confirms there is no structural change from spinel itself (data not shown) thus the different cycling stabilities should originate from the graphene with different number of functional groups.

EIS technique was then adopted to study the impedance evolution of spinel electrodes with different graphenes at different states of charge (SOC). As shown in Fig. 5, the high-frequency arc is an indication of the resistance and capacitance from the particle-to-particle contacts in the electrode, which is also closely related with the Li^+ ion transport within the surface film formed on the electrode, while the medium-frequency arc is associated with the charge transfer resistance [33,34]. Similar particle-to-particle resistances are observed in fresh electrodes containing different graphenes. However, when charged to high voltage, the electrode with graphene14 shows much faster increase of particle-to-particle resistance, which is ~2500 Ω at 5.0 V (~10 times of that for

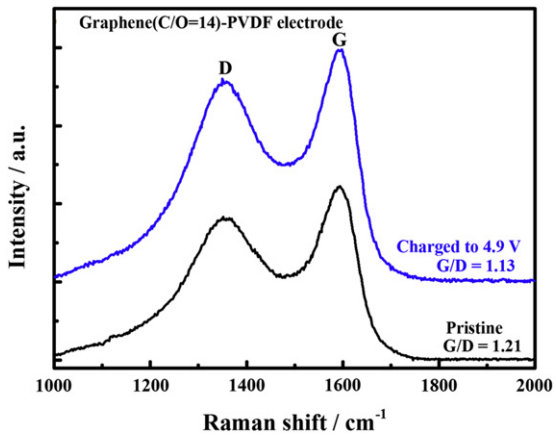

Fig. 6. Raman spectra of graphene (C/O = 14)-PVDF electrode before charge and at charged state of 4.9 V.

electrode with graphene100). This high resistance also reflects the surface film that formed between individual particles during charging. The primary difference between graphene14 and graphene100 is the content of oxygen containing functional groups. Therefore, it could be inferred that more functional groups have been oxidized at high voltage on graphene14 than on graphene100, leading to a thicker surface film resistance and deteriorating the electrical conductivity of the whole electrode. Accordingly, capacity degradation is accelerated on graphene14 during cycling.

To further confirm the structural change of graphene14 during charge to high voltage, Raman spectra of graphene14-PVDF electrodes before charge and at charged state of 4.9 V were measured and the data are shown in Fig. 6. The peaks located at ca. 1352 and 1592 cm^{-1} correspond to the D and G bands of graphene, respectively. The D band is associated with the disorder induced in sp^3 carbon (C–C), while the G bands arise from the in-plane vibration of sp^2 carbon (C=C). When the electrode with graphene14 is charged to 4.9 V, the relative intensity ratio of G/D decreases from 1.21 to 1.13, revealing a loss of conducting C=C double bond. It is speculated that the transition of carbon hybridization from sp^2 to sp^3 dramatically lowers the electrical conductivity of graphene14.

The above discussion demonstrates that an increased amount of functional groups on graphene surface leads to lower Coulombic efficiency and faster capacity degradation. In other words, during high voltage operation, electrolyte decomposition and oxidation of functional groups occur simultaneously on carbon surfaces. Therefore in practical applications, while the surface area of carbon

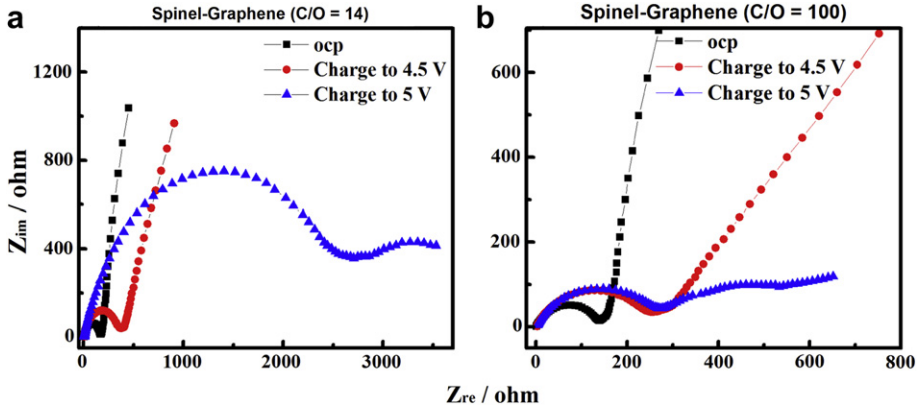

Fig. 5. EIS spectra of spinel electrodes with different graphenes measured at different charged states: open circuit potential (ocp), charged states of 4.5 V and 5.0 V.

can be chosen according to different system requirements, the functional groups should be minimized when operated at high voltages [35].

4. Conclusions

The electrochemical properties of different carbon additives at high voltages have been systematically investigated. Large surface area of carbon additive leads to deteriorated initial Coulombic efficiency and cycling stability due to the electrolyte decomposition. However, the intrinsic reasons of the parasitic reactions are different for various carbons. SP or AB with low surface areas demonstrates certain intercalation properties that allow PF_6^- to reversibly diffuse in/out at above 4.8 V. For KB and graphene, surface functional groups are concurrently oxidized at high voltages in addition to the decomposition of electrolyte, generating a thick passivation film on the electrode surface and deteriorating the cell performances. A careful selection of carbon additive is critical to maximize the cell performances by reducing the undesired side reactions for high voltage systems.

Acknowledgments

This work was supported by the Assistant Secretary for Energy Efficiency and Renewable Energy, Office of Vehicle Technologies of the U.S. Department of Energy under Contract No. DE-AC02-05CH11231, Subcontract No 18769 under the Batteries for Advanced Transportation Technologies (BATT) Program. Scanning electron microscopy and Raman spectra measurements was conducted in the William R. Wiley Environmental Molecular Sciences Laboratory (EMSL), a national scientific user facility sponsored by DOE's Office of Biological and Environmental Research and located at PNNL. We thank Drs. Dehong Hu (EMSL) and Xiaolin Li (PNNL) for their help on Raman and XRD tests, respectively.

References

[1] M.E. Spahr, D. Goers, A. Leone, S. Stallone, E. Grivei, J. Power Sources 196 (2011) 3404.
[2] G. Liu, H. Zheng, A.S. Simens, A.M. Minor, X. Song, V.S. Battaglia, J. Electrochem. Soc. 154 (2007) A1129.
[3] J. Xiao, X. Chen, P.V. Sushko, M.L. Sushko, L. Kovarik, J. Feng, Z. Deng, J. Zheng, G.L. Graff, Z. Nie, D. Choi, J. Liu, J.-G. Zhang, M.S. Whittingham, Adv. Mater. 24 (2012) 2109.
[4] L. Xiao, Y. Cao, J. Xiao, W. Wang, L. Kovarik, Z. Nie, J. Liu, Chem. Commun. 48 (2012) 3321.
[5] M.G. Lazarraga, S. Mandal, J. Ibañez, J.M. Amarilla, J.M. Rojo, J. Power Sources 115 (2003) 315.
[6] J. Xiao, D. Wang, W. Xu, D. Wang, R.E. Williford, J. Liu, J.-G. Zhang, J. Electrochem. Soc. 157 (2010) A487.
[7] S. Kuroda, N. Tobori, M. Sakuraba, Y. Sato, J. Power Sources 119–121 (2003) 924.
[8] C.-C. Chang, L.-J. Her, H.-K. Su, S.-H. Hsu, Y.T. Yen, J. Electrochem. Soc. 158 (2011) A481.
[9] N. Zhu, W. Liu, M. Xue, Z. Xie, D. Zhao, M. Zhang, J. Chen, T. Cao, Electrochim. Acta 55 (2010) 5813.
[10] D. Wang, D. Choi, J. Li, Z. Yang, Z. Nie, R. Kou, D. Hu, C. Wang, L.V. Saraf, J. Zhang, I.A. Aksay, J. Liu, ACS Nano 3 (2009) 907.
[11] C. Venkateswara Rao, A. Leela Mohana Reddy, Y. Ishikawa, P.M. Ajayan, ACS Appl. Mater. Interfaces 3 (2011) 2966.
[12] P. Meduri, H. Chen, X. Chen, J. Xiao, M.E. Gross, T.J. Carlson, J.-G. Zhang, Z.D. Deng, Electrochem. Commun. 13 (2011) 1344.
[13] K. Zaghib, J. Shim, A. Guerfi, P. Charest, K.A. Striebel, Electrochem. Solid-State Lett. 8 (2005) A207.
[14] M. Kunduraci, J.F. Al-Sharab, G.G. Amatucci, Chem. Mater. 18 (2006) 3585.
[15] K.M. Shaju, P.G. Bruce, Dalton Trans. (2008) 5471.
[16] W. Xu, X. Chen, F. Ding, J. Xiao, D. Wang, A. Pan, J. Zheng, X.S. Li, A.B. Padmaperuma, J.-G. Zhang, J. Power Sources 213 (2012) 304.
[17] J. Zheng, J. Xiao, X. Yu, L. Kovarik, M. Gu, F. Omenya, X. Chen, X.-Q. Yang, J. Liu, G.L. Graff, M.S. Whittingham, J.-G. Zhang, Phys. Chem. Chem. Phys. 14 (2012) 13515.
[18] X. Chen, W. Xu, J. Xiao, M.H. Engelhard, F. Ding, D. Mei, D. Hu, J. Zhang, J.-G. Zhang, J. Power Sources 213 (2012) 160.
[19] J.A. Seel, J.R. Dahn, J. Electrochem. Soc. 147 (2000) 892.
[20] T. Ishihara, M. Koga, H. Matsumoto, M. Yoshio, Electrochem. Solid-State Lett. 10 (2007) A74.
[21] G. Li, D. Hu, G. Xia, J.M. White, C. Zhang, Rev. Sci. Instrum. 79 (2008) 074101.
[22] J. Xiao, D. Mei, X. Li, W. Xu, D. Wang, G.L. Graff, W.D. Bennett, Z. Nie, L.V. Saraf, I.A. Aksay, J. Liu, J.-G. Zhang, Nano Lett. 11 (2011) 5071.
[23] J.-G. Zhang, D. Wang, W. Xu, J. Xiao, R.E. Williford, J. Power Sources 195 (2010) 4332.
[24] J. Xiao, J. Hu, D. Wang, D. Hu, W. Xu, G.L. Graff, Z. Nie, J. Liu, J.-G. Zhang, J. Power Sources 196 (2011) 5674.
[25] W. Xu, V.V. Viswanathan, D. Wang, S.A. Towne, J. Xiao, Z. Nie, D. Hu, J.-G. Zhang, J. Power Sources 196 (2011) 3894.
[26] D.H. Jang, Y.J. Shin, S.M. Oh, J. Electrochem. Soc. 143 (1996) 2204.
[27] S.S. Zhang, T.R. Jow, J. Power Sources 109 (2002) 172.
[28] W. Märkle, N. Tran, D. Goers, M.E. Spahr, P. Novák, Carbon 47 (2009) 2727.
[29] H.F. Xiang, X. Zhang, Q.Y. Jin, C.P. Zhang, C.H. Chen, X.W. Ge, J. Power Sources 183 (2008) 355.
[30] H. Lee, S. Choi, S. Choi, H.-J. Kim, Y. Choi, S. Yoon, J.-J. Cho, Electrochem. Commun. 9 (2007) 801.
[31] J. Hassoun, S. Panero, P. Reale, B. Scrosati, Adv. Mater. 21 (2009) 4807.
[32] K.N. Kudin, B. Ozbas, H.C. Schniepp, R.K. Prud'homme, I.A. Aksay, R. Car, Nano Lett. 8 (2008) 36.
[33] Z. Liu, J.Y. Lee, H.J. Lindner, J. Power Sources 97–98 (2001) 361.
[34] D. Zhang, B.S. Haran, A. Durairajan, R.E. White, Y. Podrazhansky, B.N. Popov, J. Power Sources 91 (2000) 122.
[35] R. Kostecki, T. Richardson, U.S. DOE Hydrogen and Fuel Cells Program and Vehicle Technologies Program Annual Merit Review (AMR), 2012. es033.